

Effect of Tool Pin Geometry on the Mechanical Properties of Friction Stir Welded AA5083 composites

Prabhu L^{1}, Deepak R², George Antony Casmir³ & Selvababu B³*

¹ Professor, Department of Mechanical Engineering, Aarupadai Veedu Institute of technology, Vinayaka Mission's Research foundation, Salem, TamilNadu

² PG Scholar, Department of Mechanical Engineering, Aarupadai Veedu Institute of technology, Vinayaka Mission's Research foundation, Salem, TamilNadu

³ Assistant Professor, Department of Mechanical Engineering, Aarupadai Veedu Institute of technology, Vinayaka Mission's Research foundation, Salem, TamilNadu

Abstract. This research examined three distinct tool pin geometries of friction stir weld of AA 5083-T6 to determine the optimal shape for final weld characteristics. The tool traverse speed and tool rotational speed were considered as input process factors. A hybrid methodology combining Multi-Objective Optimization on Basis of Ratio Analysis with Entropy technique was presented to achieve optimal values of parameters that concurrently enhance yield strength, ultimate tensile strength, hardness, and elongation. A comparison of the optimum outcomes for all tool geometries indicates that the Taper threaded (TT) tool exhibits superior qualities (YS-142 MPa, UTS-271 MPa, hardness-87 HV0.1, percentage elongation-16.92%) compared to the other two tools. For TT, enhancements of 22.68% and 11.45% at UTS were noted in comparison to cylindrical threaded (CT) tool and Taper (T) tools. The Taper threaded tool exhibits the maximum torque, X-force, and Z-force when evaluated against other tools under optimal parameters. An enhancement of 16.07% and 2.37% at torque values is observed for the Taper threaded tool in comparison to the cylindrical threaded tool and T tool. Fluctuation at Z-force were observed with the cylindrical threaded tool. The distribution of X-force was relatively more uniform and stable for Taper threaded. A greater degree of X-force variation was noted for Taper tool. The coefficients of friction for T, Taper threaded, and cylindrical threaded tool are 0.242, 0.227, and 0.370, respectively. Confirmation tests were conducted to validate optimized parameters for all instruments, which were confirmed to be within acceptable limits. Moreover, enhanced force and torque performance was achieved using the tapered threaded tool.

1. Introduction

FSW has emerged as most effective joining procedures for various grades of aluminum alloy, occurs in a solid state. FSW parameters for AA5083/MgAZ31B joints, finding optimal conditions lead to improved tensile strength and impact energy. Intermetallic compounds increase micro hardness, highlighting FSW's potential for high-strength, lightweight material

* Corresponding author: prablogu@gmail.com

applications [1]. The impact of tool-pin geometries (tri-flute, double-flute, non-fluted) is evident on the mechanical characteristics of AA5083 welds. The tri-fluted tool demonstrates exceptional tensile strength, elongation, and consistent hardness, hence improving weld quality for structural applications [2]. The influence of process parameters on FSW of dissimilar AA5083 and AA6061 alloys is significant. The findings indicate that proper welding conditions enhance tensile strength and microstructure, guaranteeing defect-free, high-quality joints appropriate for maritime applications [3]. FSW on dissimilar AA5083–AA6082 joints, revealing FSW superior tensile strength. These findings suggest FSW suitability for applications requiring high mechanical strength [4]. The thermal and mechanical properties of FSW AA5083 composites reinforced with SiC and B4C is significant. Hybrid reinforcement significantly improves tensile strength, fatigue life, and hardness, while balancing strength and fracture toughness for aerospace and automotive use [5]. Post-processing intervals between friction stir processing and TIG welding of AA5083 joints influences effective result. Reduced time intervals enhance ultimate tensile strength and hardness, optimizing mechanical performance for improved weld quality [6]. FSW of distinct AA5083-H111 and AA6106-T6 joints aims to identify optimal welding settings resulting in enhanced hardness and tensile strength. Optimal mechanical qualities are attained through meticulous regulation of rotational speed, welding speed, and tool plunge depth [7]. Taguchi method is applied to optimize Friction Stir Processing parameters for AA5083/Coal composites. The optimal process parameters values are tool tilt angle of 2° , a rotating speed of 900 rpm, and a traverse speed of 60 mm/min, resulting in enhanced mechanical characteristics [8]. Machine learning concept is applied to forecast the ultimate tensile strength (UTS) of friction stir welded AA7075/AA5083 joints. The Decision Tree model surpassed others, attaining 97% accuracy in forecasting UTS, hence improving the welding process efficiency [9]. Taguchi method is applied to optimise the Parameters for Friction Stir Processing (FSP) of AA5083/SiC composites. The findings indicate that the ideal settings (tool tilt angle of 2° , rotational speed of 900 rpm, and traverse speed of 30 mm/min) yield maximum tensile strength and microhardness [10]. Taguchi L9 method is used to optimise the Friction Stir Welding (FSW) parameters for AA5083-AA6063 alloy joints. The ideal settings yielded a tensile strength of 215.40 MPa and a hardness of 90.69 HV, with rotation speed identified as the most significant factor [11]. The parameters for AA6063-T6 and AA5083-H32 alloys joint is optimized for UFSW process. The optimal parameters improve tensile strength, yield strength, and elongation with spindle speed having the most significant impact on mechanical properties [12]. The optimization of Parameters for friction stir welding (FSW) of AA5083-O and AA6082-T6 alloys utilizing Gray Relational Analysis (GRA), Principal Component Analysis (PCA) and Response Surface Methodology (RSM) was carried out. The ideal settings of 1900 rpm, 40 mm/min, and a 12 mm shoulder diameter enhance tensile strength, elongation, yield strength, dome height, and micro hardness [13]. Friction Stir Welding (FSW) was optimized for AA2014-T6 and AZ31B alloys using Taguchi method for tensile strength, micro hardness and elongation. The stepped square pin profile, 1000 rpm rotation speed, and 60 mm/min welding speed yielded maximum mechanical properties, outperforming conventional methods [14]. The impact of tool pin profiles (circular, triangular, square) on the mechanical properties of AA3103 alloy welds was studied. The circular pin profile showed the best balance of ultimate tensile strength, elongation, and microstructure, making it ideal for high-quality FSW joints [15]. FSW parameters is optimised for AA5083 alloy joints using Taguchi L9 and VIKOR methods. The best results were achieved with a concave tool profile, 1400 rpm rotational speed, and 40 mm/min welding speed, improving tensile strength, elongation, and microhardness [16]. The influence of rotational and travel speeds is more evident on the tensile strength and microstructure characteristics for the friction stir welding of AA6063-T4 and AZ31B magnesium alloys. The optimal parameters identified were 1120 rpm and 63 mm/min,

resulting in enhanced tensile strength and microhardness [17]. Underwater friction stir welding (UFSW) of SiC-reinforced A356 aluminum alloys using a hybrid CoCoSO and MERE approach was studied. The optimal parameters like welding speed (0.57 mm/s), rotational speed (1300 rpm), axial force (6000 N), and SiC content (8 wt%) significantly enhances tensile strength, elongation, and yield strength [18]. Friction stir additive manufacturing (FSAM) is used for developing Metal matrix composites (MMCs). The process improves microstructure by integrating metallic and ceramic nanoparticles, enhancing hardness, friction, and durability, making them ideal for aviation applications requiring radiation shielding and high-temperature durability [19]. The wear behavior of AA5052/B4C metal matrix composites (MMCs) is studied using artificial neural networks (ANN). The results reveal that wear resistance improves with increased reinforcement volume and particle size ratio, but excessive reinforcement volume can reduce wear resistance due to dislodged particles [20]. This study primarily focuses on multi-objective optimization of FSW of AA 5083-T6 using various tools, accounting for differing traverse speeds and tool rotational. The aim of this study is to identify the optimal tool geometry by comparing the optimized outcomes from individual trials done for each tool geometry in the collection. A hybrid methodology, namely MOORA combined with Entropy is utilized to identify the optimal welding parameters for all tool. Consequently, challenge of integrating categorical variable (tool geometry) into design matrix alongside numeric values were circumvented. Furthermore, focusing solely on the optimum findings for final analysis will diminish the work required by limiting the number of specimens to be examined. An in-depth examination of torque and force distribution, along with SEM analysis of the optimal parameters will facilitate selection of the most suitable tool shape.

2. Materials and methodology

The three tool geometries shown in Figure 1 are predominantly used for friction stir welding due to their relative ease of fabrication, attributed to their uncomplicated geometrical characteristics. Furthermore, the choice of these three tool geometries enables a systematic examination of the impact of variations in tool pin shape. The initial tool were taper tool (T). The second kind were the taper threaded tool, which might be considered a version of the taper tool, including threads integrated into surface of truncated cone. It is evident from the study that thread often enhances material flow. The alteration in pin size will also modify effective tool-workpiece volume. Consequently, choice of tool pin geometries facilitates analysis on the impact of dimensions and pin shape including thread.

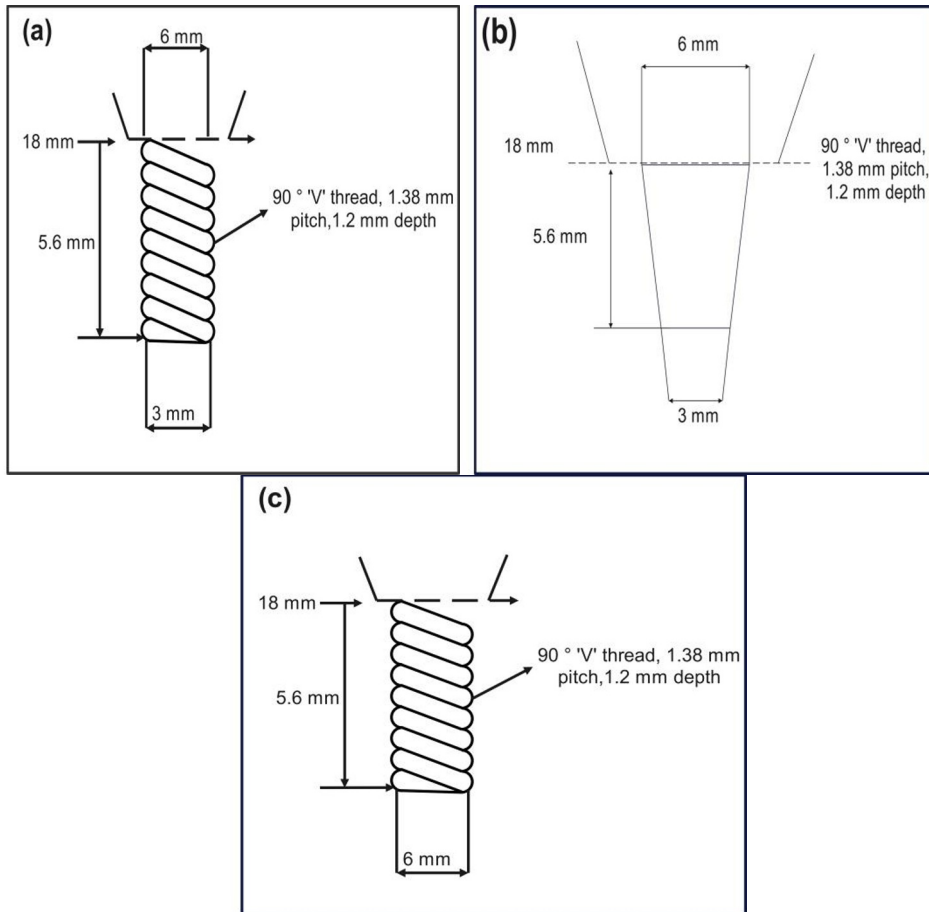


Fig. 1. Tool pin dimensions: 'V' thread 90°, pitch 1.38 mm, depth 1.2 mm, tool radius 0.1 mm

AA 5083-T6, measuring 150 × 65 × 6 mm were utilized at investigation of butt joint design with weld length of 120 mm. Tables 1–3 present the chemical composition and mechanical characteristics of the composites.

Table 1 Chemical composition of AA 5083-T6.

Chemical composition (Wt %)	Fe	Si	Cr	Cu	Mn	Mg	Al
	0.4	0.4	0.8	0.1	0.4	4.0	Bal.

Table 2 Mechanical characteristics of AA 5083-T6.

Characteristics	YS	UTS	Hardness	Percentage elongation
Values	310MPa	350 MPa	120	16%

Table 3 DOE for investigation.

S.No	A: TRS (rpm)	B: TTS (mm/sec)
1	800	1.00

2	800	1.50
3	800	2.00
4	1200	1.00
5	1200	1.50
6	1200	2.00
7	1600	1.00
8	1600	1.50
9	1600	2.00

The TPG (Tool Pin Geometry), TRS (Tool Rotational Speed) and TTS (Tool traverse speed), were changed at three stages. Preliminary experiments were undertaken based on existing literature to ascertain the viable operational ranges of all input variable. Additionally, variable limitations was assessed by examining the weldment for a uniform appearance and the absence of apparent faults. The TRS and TTS are adjusted at three levels, utilizing complete factorial design of experiments for the experimental design (Table 3). All studies were performed using 3-Ton linear Friction Stir Welding machine in a fixed Z-axis mode. Machine possesses maximum 10 kN thrust on the X-axis and capacity of 30 kN thrust on the Z-axis. Spindle speed may be adjusted indefinitely 3000 RPM. The machine's spindle torque were 85 N·m at 1600 RPM. Experiment involves measuring forces and torque using strain gauge, interfaced with PLC system. Upon completion of welding, samples were prepared for tensile testing in accordance with ASTM E8 and evaluated on strain rate. The hardness were measured in the center of nugget within a 5 x 5 mm area with a total of 50 points assessed at 0.5 mm intervals [21]. Hardness were assessed using 100 gf force and a 10-second dwell period at many locations with average values were computed.

2.1. Optimization

The identification of the optimal combination in welding were formidable challenge due to the multitude of responses and input process parameters obtained from multi-level trials. In industry, ideal values of quality attributes were approximately established based on practical data management and operator performance literature. The aforementioned hybrid technique, namely Multi-Objective Optimization on Basis of Ratio Analysis method combined with Entropy were prioritized for implementation to alleviate issues.

2.1.1. Optimizing FSW with Entropy and MOORA

Entropy-based MCDM and MOORA are robust methodologies employed for mass determination at multi-criteria decision-making. Entropy measures the uncertainty associated with each criteria, attributing greater significance to those exhibiting larger data variability, thus rendering it suitable for managing uncertain data. MOORA simplifies intricate multi-objective issues by normalizing criterion values and use ratio analysis to rank alternatives. Combined entropy yields objective weights derived from data variability, whereas MOORA use these weights to assess and rank alternatives, hence providing optimal decision-making through the equilibrium of all criteria. This hybrid methodology is very efficacious in optimizing intricate processes, such as FSW tool geometry, when several competing objectives are present.

2.1.2. Weights of Indexes

The entropy weighting method is used in this study to determine the index weights. The entropy weight technique determines weights based on information quantity by automatically solving mathematical models, without regard for the decision maker's input. The weight index of each machining feature is calculated using the following processes derived from the study results.

Decision Matrix Structure is formed based on the following method. If evaluation set of multi attribute decision-making were $M = (M_1, M_2, \dots, M_m)$, index set were $N = (N_1, N_2, \dots, N_n)$, and j th index's value at i th alternative were x_{ij} ; then, decision matrix is $X = [x_{ij}]_{m \times n}$.

Decision Matrix Standardization: To mitigate impact of index dimensions and their variable range at assessment outcomes were essential to normalize original matrix to maintain uniformity and equivalence across all characteristics; subsequently, normalized decision matrix were

$$Y = (y_{ij})_{m \times n}, \quad i = 1, 2, \dots, m; j = 1, 2, \dots, n \quad (1)$$

$$y_{ij} = \frac{x_{ij}}{\sum_{i=1}^m x_{ij}}, \quad i = 1, 2, \dots, m; j = 1, 2, \dots, n$$

Computation of the Index's Entropy. The entropy of j th index were defined as

$$e = -k \sum_{i=1}^m y_{ij} \ln(y_{ij}), \quad 0 \leq e \leq 1 \quad (2)$$

wherein: $k = (\ln(m))^{-1}$, ($i = 1, 2, \dots, m; j = 1, 2, \dots, n$)

Computation of Entropy mass of Index. The entropy mass of j th index were ascertained by

$$w_j = \frac{h_j}{\sum_{j=1}^n h_j}, \quad j = 1, 2, \dots, n \quad (3)$$

wherein: $h_j = 1 - e_j$

2.2. Multi-Objective Optimization on the Basis of Ratio Analysis (MOORA)

The MOORA technique is the multi-criteria decision-making strategy utilized to select the optimal alternatives from a finite collection of accessible options. This technique employs both favorable (maximizing) and non-beneficial (minimization) factors to provide optimal selections while eliminating inappropriate criteria to enhance the selection process. MOORA optimizes multiple conflicting objectives by converting them into a single optimal solution through ratio-based comparisons [22]. The MOORA technique requires fewer computations and exhibits more robustness; it may simultaneously address several criteria, provide almost precise rankings of material alternatives, and support ratio system approach. The ranks generated using two methodologies were compared. This method commences with decision matrix which enumerates many options in accordance with multiple criterion. The subsequent text outlines the processes of the MOORA ratio system:

Step 1: Creation of decision matrix ' X ' entails positioning the i^{th} indicators which evaluate significance of options based on the j^{th} criterion. The choice matrix is represented as $X = [x_{ij}]_{m \times n}$

Step 2: Decision matrix were normalized via Equation 4.

$$\hat{x}_{ij} = \frac{x_{ij}}{\sqrt{\sum_{j=1}^n x_{ij}^2}} \quad (4)$$

Step 3: The weighted and normalized decision matrix was derived using Eqn 4. The weight assigned to j^{th} criteria may be deduced from value of w_j . The mass can be calculated via entropy method or the entropy methodology. This study use the entropy approach to calculate weight estimations.

$$V_i = W_j x \hat{X}_{ij} \quad (5)$$

Step 4: Final preference values, (\tilde{y}_i) ., derived from Eqn 16. Here, $j = 1, 2, \dots, g$ denotes criterion to be maximized,

$$\tilde{y}_i = \sum_{j=1}^g v_{ij} - \sum_{j=g+1}^g v_{ij} \quad (6)$$

Step 5: The ranking of alternatives were established using ordering the y_i . Values ranges from highest to lowest.

3. Results and discussion

The L9, orthogonal array with output results for Taper (T), Taper threaded (TT), cylindrical threaded (CT) tools, is shown in Tables 4–6, respectively. The T tool exhibits peak values of UTS at 192 MPa, YS at 134 MPa, % EL at 16.44%, and hardness at 81 Hv0.1, attained at 1200 RPM and 1.5 mm/sec. The taper threaded tool exhibits maximum values of YS, UTS, hardness, and % EL at 142 MPa, 217 MPa, 87 HV and 16.92%, 0.1 (1200 RPM, 2.00 mm/sec). The cylindrical threaded tool achieves maximum of 191 MPa (1200 RPM, 2.00 mm/sec) for ultimate tensile strength (UTS), 123 MPa (800 RPM, 2.00 mm/sec) for yield strength (YS), 10.4% (1200 RPM, 2.00 mm/sec) for percentage elongation (% El), and 80 Hv0.1 (800 RPM, 1.00 mm/sec) for hardness as detailed in Table 6.

Table 4 Quality characteristics decision matrix (T Tool).

No.	UTS	YS	% El	Hardness	Torque	X-Force	Z-Force
1	169	95	6.54	55	14.53	1092	8779
2	190	119	9.88	62	19.64	1517	9566
3	179	102	9.37	57	20.22	1339	8510
4	178	115	9.96	69	10.86	1156	5220
5	199	134	16.44	81	12.07	1348	5051
6	188	119	15.35	74	12.55	1390	7346
7	177	104	6.29	65	10.24	1110	4984
8	195	118	8.45	73	10.58	1243	4430
9	180	109	9.37	69	10.94	1267	6415

Table 5 Quality characteristics decision matrix (TT Tool).

No.	UTS	YS	% El	Hardness	Torque	X-Force	Z-Force
1	194	117	12.98	75	17.09	1320	10172
2	206	135	14.45	84	21.87	1469	10749
3	216	134	15.44	86	14.51	1512	9222

4	179	95	11.46	74	12.39	1367	7350
5	201	126	14.58	82	13.96	1460	6908
6	217	142	16.92	87	22.50	1839	7639
7	160	89	7.74	69	11.54	1321	7072
8	172	98	8.4	70	11.26	1391	6509
9	200	125	11.47	73	12.55	1360	7811

Table 6 Quality characteristics decision matrix (CT Tool)

No.	UTS	YS	% El	Hardness	Torque	X-Force	Z-Force
1	176	109	8.5	80	14.24	1298	5712
2	179	107	8.9	73	20.53	1324	11430
3	155	123	7.4	74	21.63	1273	5798
4	118	81	6.6	68	11.21	1157	3989
5	127	87	6.8	72	12.57	1240	4841
6	191	118	10.4	74	21.55	1218	9982
7	114	104	6.2	61	10.78	1116	3885
8	108	97	6.4	71	11.03	1174	4397
9	136	88	6.9	71	12.73	1207	5382

The comparison indicates that the Taper threaded tool achieves optimal mechanical characteristics. In addition to mechanical qualities, the assessment of forces and torque generated by all tool were crucial criterion, especially regarding the tool's lifetime. Reduced forces and increased torque can enhance plastic deformation while exerting less stress on tools with the optimization of characteristics also being a key factor. These factors complicate selection of a process parameters and appropriate instrument. This inquiry examines input process factors including TS, TRS, and TTS, while the responses measured include yield strength (YS), ultimate tensile strength (UTS), hardness (Hv), percentage elongation (%EL), torque, Z-force, and X-force of the weld nugget. Quality qualities may be categorized into three types: lower is preferable, greater is preferable and nominal is preferable. The primary objective to enhance mechanical qualities of the welded joint. For torque, X-force, and Z-force, a signal-to-noise ratio exhibiting a 'smaller the better' characteristic is preferable.

3.1. Optimal process parameter evaluation for T tool

The S/N ratio for different output was computed by Minitab 20, as presented at Table 7.

Table 7 S/N ratio for T tool results.

S.No	UTS	YS	El	HV	Torque	X-Force	Z-Force
1	44.56	39.55	16.31	34.81	-23.25	-60.76	-78.87
2	45.58	41.51	19.90	35.85	-25.86	-63.62	-79.61
3	45.06	40.17	19.43	35.12	-26.12	-62.54	-78.60
4	45.01	41.21	19.97	36.78	-20.72	-61.26	-74.35
5	45.98	42.54	24.32	38.17	-21.63	-62.59	-74.07
6	45.48	41.51	23.72	37.38	-21.97	-62.86	-77.32
7	44.96	40.34	15.97	36.26	-20.21	-60.91	-73.95

8	45.80	41.44	18.54	37.27	-20.49	-61.89	-72.93
9	45.11	40.75	19.43	36.78	-20.78	-62.06	-76.14

A study compares FSW was found to be the most sustainable welding process based on environmental, economic, and social factors, optimized by entropy-weighted MCDM methods [23]. The findings are presented in Table 8.

Table 8. Entropy weight results

	UTS	YS	EI	HV	Torque	X-Force	Z-Force
W_j	0.003	0.014	0.615	0.027	0.302	0.007	0.032

The process starts with formulation of choice matrix presented at Table 4. The values was standardized in accordance with Equation 4, as seen in Table 9.

Table 9. Normalized decision matrix using MOORA

S.No	UTS	YS	EI	HV	Torque	X-Force	Z-Force
1	0.328	0.322	0.273	0.318	-0.345	-0.326	-0.345
2	0.336	0.337	0.333	0.327	-0.384	-0.342	-0.348
3	0.332	0.327	0.325	0.321	-0.388	-0.336	-0.344
4	0.331	0.335	0.334	0.336	-0.308	-0.329	-0.325
5	0.338	0.346	0.407	0.349	-0.321	-0.336	-0.324
6	0.335	0.337	0.397	0.341	-0.326	-0.338	-0.338
7	0.331	0.328	0.267	0.331	-0.3	-0.327	-0.323
8	0.337	0.337	0.31	0.34	-0.304	-0.332	-0.319
9	0.332	0.331	0.325	0.336	-0.309	-0.333	-0.333

The entropy technique was employed to obtain mass for each criteria (Table 3). According to eqn 5, weighted normalized values were computed and displayed in Table 10. Subsequently, equation 6 is employed to assess the final preference values, which are presented in Table 10.

Table 10. Weighted Normalization and Preference Value (\tilde{y}_i) with rank.

S.No	UTS	YS	EI	HV	Torque	X-Force	Z-Force	\tilde{y}_i	Rank
1	0.00098	0.0045	0.1679	0.0086	-0.1043	-0.0023	-0.0110	0.2996	8
2	0.00101	0.0047	0.2048	0.0088	-0.1160	-0.0024	-0.0111	0.3489	3
3	0.00100	0.0046	0.2001	0.0087	-0.1172	-0.0024	-0.0110	0.3448	4
4	0.00099	0.0047	0.2055	0.0091	-0.0929	-0.0023	-0.0104	0.3259	5
5	0.00102	0.0048	0.2504	0.0094	-0.0971	-0.0024	-0.0104	0.3754	1
6	0.00100	0.0047	0.2442	0.0092	-0.0986	-0.0024	-0.0108	0.3709	2

7	0.00099	0.0046	0.1644	0.0089	-0.0907	-0.0023	-0.0104	0.2822	9
8	0.00101	0.0047	0.1908	0.0092	-0.0919	-0.0023	-0.0102	0.3102	7
9	0.00100	0.0046	0.2001	0.0091	-0.0932	-0.0023	-0.0107	0.321	6

Ultimately, Table 11 presents the materials ranked by their preference values. The table indicates S.No. 5 is ranked first with preference value of 0.3754, while s.no. 7 is ranked ninth with preference value of 0.2822.

3.2. Optimal process parameter evaluation for TT tool

Likewise, the signal-to-noise ratio for output responses of the Taper threaded tool was computed using Minitab 20, as seen at Table 11.

Table 11 S/N ratio for Taper threaded Tool results.

S.No	UTS	YS	EI	HV	Torque	X-Force	Z-Force
1	45.76	41.36	22.27	37.50	-24.65	-62.41	-80.15
2	46.28	42.61	23.20	38.49	-26.80	-63.34	-80.63
3	46.69	42.54	23.77	38.69	-23.23	-63.59	-79.30
4	45.06	39.55	21.18	37.38	-21.86	-62.72	-77.33
5	46.06	42.01	23.28	38.28	-22.90	-63.29	-76.79
6	46.73	43.05	24.57	38.79	-27.04	-65.29	-77.66
7	44.08	38.99	17.77	36.78	-21.24	-62.42	-76.99
8	44.71	39.82	18.49	36.90	-21.03	-62.87	-76.27
9	46.02	41.94	21.19	37.27	-21.97	-62.67	-77.85

The entropy weights are determined based on equations (1) – (3). The findings are presented in Table 12.

Table 12. Entropy weight results

	UTS	YS	EI	HV	Torque	X-Force	Z-Force
W _j	0.017	0.055	0.498	0.018	0.388	0.008	0.016

The process starts with formulation of selection matrix presented at Table 4. The values was standardized in accordance with equation 4, as presented in table 13.

Table 13. Normalized decision matrix using MOORA

S.No	UTS	YS	EI	HV	Torque	X-Force	Z-Force
1	0.3336	0.3335	0.3396	0.3308	-0.3495	-0.3293	-0.342
2	0.3374	0.3435	0.3538	0.3394	-0.3799	-0.3342	-0.344
3	0.3404	0.343	0.3625	0.3412	-0.3294	-0.3355	-0.3384

4	0.3285	0.3189	0.3231	0.3297	-0.3099	-0.3309	-0.3299
5	0.3359	0.3387	0.355	0.3376	-0.3246	-0.3339	-0.3276
6	0.3407	0.3471	0.3747	0.3421	-0.3834	-0.3445	-0.3314
7	0.3214	0.3144	0.2711	0.3244	-0.3012	-0.3293	-0.3285
8	0.326	0.3211	0.2819	0.3255	-0.2981	-0.3317	-0.3254
9	0.3355	0.3381	0.3232	0.3287	-0.3115	-0.3306	-0.3322

The entropy technique was employed to obtain weights for each criteria (Table 3). According to eqn 5, weighted normalized values were computed and displayed in Table 14. Subsequently, equation 6 is employed to assess the final preference values, which are presented in Table 14.

Table 14. Weighted Normalization and Preference Value (\hat{y}_i) with rank.

S. No	UTS	YS	EI	HV	Torque	X-Force	Z-Force	\hat{y}_i	Rank
1	0.0056 7	0.018 34	0.1691	0.0059 5	-0.13561	-0.00263	-0.00547	0.3428	4
2	0.0057 4	0.018 89	0.1761 7	0.0061 1	-0.1474	-0.00267	-0.0055	0.3625	2
3	0.0057 9	0.018 87	0.1805 5	0.0061 4	-0.1278	-0.00268	-0.00541	0.3472	3
4	0.0055 8	0.017 54	0.1608 8	0.0059 4	-0.12025	-0.00265	-0.00528	0.3181	7
5	0.0057 1	0.018 63	0.1767 7	0.0060 8	-0.12595	-0.00267	-0.00524	0.3410	5
6	0.0057 9	0.019 09	0.1865 8	0.0061 6	-0.14875	-0.00276	-0.0053	0.3744	1
7	0.0054 6	0.017 29	0.1349 9	0.0058 4	-0.11685	-0.00263	-0.00526	0.2883	9
8	0.0055 4	0.017 66	0.1403 9	0.0058 6	-0.11568	-0.00265	-0.00521	0.2930	8
9	0.0057	0.018 6	0.1609 4	0.0059 2	-0.12086	-0.00265	-0.00532	0.3200	6

Ultimately, Table 11 illustrates the materials sorted by their preference ranges. It is evident from the table that S.No 6 is rated first with preference of 0.3744, while S.no. 7 is ranked ninth with preference of 0.2883.

3.3. Optimal process parameter evaluation for CT tool

Likewise, the S/N ratio for output of the cylindrical threaded tool was computed using Minitab 20, as shown at Table 15.

Table 15 S/N ratio for cylindrical threaded tool results.

S.No	UTS	YS	EI	HV	Torque	X-Force	Z-Force
------	-----	----	----	----	--------	---------	---------

1	44.91	40.75	18.59	38.06	-23.07	-62.27	-75.14
2	45.06	40.59	18.99	37.27	-26.25	-62.44	-81.16
3	43.81	41.80	17.38	37.38	-26.70	-62.10	-75.27
4	41.44	38.17	16.39	36.65	-20.99	-61.27	-72.02
5	42.08	38.79	16.65	37.15	-21.99	-61.87	-73.70
6	45.62	41.44	20.34	37.38	-26.67	-61.71	-79.98
7	41.14	40.34	15.85	35.71	-20.65	-60.95	-71.79
8	40.67	39.74	16.12	37.03	-20.85	-61.39	-72.86
9	42.67	38.89	16.78	37.03	-22.10	-61.63	-74.62

The entropy weights were calculated according to eqn (1) – (3). The results are shown in Table 16.

Table 16. Entropy weight results

	UTS	YS	EI	HV	Torque	X-Force	Z-Force
W _j	0.075	0.039	0.302	0.012	0.490	0.002	0.078

The process commences with formulation of selection matrix presented at Table 14. The values was standardized in accordance with Equation 4, as presented at Table 17.

Table 17. Normalized decision matrix using MOORA

S.No	UTS	YS	EI	HV	Torque	X-Force	Z-Force
1	0.3475	0.3390	0.3538	0.3422	-0.3289	-0.3362	-0.3329
2	0.3486	0.3376	0.3614	0.3350	-0.3742	-0.3371	-0.3596
3	0.3390	0.3477	0.3309	0.3361	-0.3807	-0.3353	-0.3335
4	0.3206	0.3175	0.3120	0.3295	-0.2993	-0.3308	-0.3191
5	0.3256	0.3227	0.3169	0.3340	-0.3135	-0.3340	-0.3265
6	0.3530	0.3447	0.3871	0.3361	-0.3803	-0.3332	-0.3544
7	0.3183	0.3356	0.3016	0.3210	-0.2945	-0.3291	-0.3181
8	0.3147	0.3305	0.3069	0.3329	-0.2973	-0.3315	-0.3228
9	0.3302	0.3235	0.3193	0.3329	-0.3151	-0.3328	-0.3306

The entropy technique was employed to obtain weights for each criterion. According to equation 5, the weighted normalized values were computed and displayed in table 18. Subsequently, equation 6 is employed to assess the final preference values, which are presented in table 18.

Table 18. Weighted Normalization and Preference Value (\tilde{y}_i) with rank.

S.No	UTS	YS	EI	HV	Torque	X-Force	Z-Force	\tilde{y}_i	Rank
1	0.0261	0.01325	0.10706	0.00411	-0.1615	-0.0007	-0.0260	0.3387	4
2	0.0262	0.01319	0.10936	0.00403	-0.1838	-0.0007	-0.0281	0.3653	2
3	0.0255	0.01359	0.10013	0.00404	-0.1869	-0.0007	-0.0261	0.3569	3
4	0.0241	0.01241	0.0944	0.00396	-0.1470	-0.0007	-0.0249	0.3074	7
5	0.0245	0.01261	0.0959	0.00402	-0.1539	-0.0007	-0.0255	0.3171	6
6	0.0265	0.01347	0.11715	0.00404	-0.1867	-0.0007	-0.0277	0.3762	1
7	0.0239	0.01311	0.09127	0.00386	-0.1446	-0.0007	-0.0249	0.3023	9
8	0.0237	0.01292	0.09286	0.00400	-0.1460	-0.0007	-0.0252	0.3053	8
9	0.0248	0.01264	0.09663	0.00400	-0.1547	-0.0007	-0.0258	0.3193	5

Ultimately, table 18 presents the materials ranked by their preference values. Table indicates that S.No. 6 is ranked first with preference value of 0.3762, while S.No.7 is ranked ninth with preference value of 0.3023.

4. Confirmatory test

Table 19 illustrates outcomes of confirmatory of all instrument under optimum parameter configuration. The observed measurements fell within acceptable boundaries of the actual ideal findings

Table 19 Conformation test results

Parameter	Optimal solution			Measured responses		
	Taper tool	Taper threaded tool	Cylindrical Threaded tool	T tool	Taper threaded tool	Cylindrical Threaded tool
1200 rpm and 2.0 mm/sec						
UTS (MPa)	199	217	191	200	221	192
YS (MPa)	134	142	118	135	143	120
%EL. (%)	16.44	16.92	10.4	17.23	18.55	10.6
Hardness (HV0.1)	81	87.26	74	81.73	87.55	72.85
Torque (N – m)	12.07	13	21.55	12.92	7.5	22.63
X-Force (N)	1348	1839	1218	1358	1879	1207
Z-force (N)	5051	7639	9982	5151	7639	10018

4.1. Heat input, torque, force, friction analysis for tool geometries

The thermal input for all tool were assessed based on derived optimum parameter configuration. Figure 2 illustrates that under comparable parameter settings T tool generates the least heat (0.73 KJ/mm), cylindrical threaded tool produces most (0.94 KJ/mm), while

the Taper threaded tool occupies a middle position (0.86 KJ/mm). Pin of the T tool is smallest of three tools; however, the inclusion of threads in the Taper threaded tool results in a greater effective contact area among workpiece and tool pin compared to T tool.

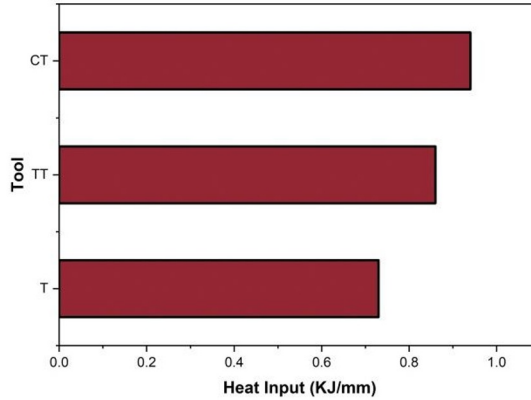


Fig. 2. Heat for tool geometries (1200 rpm, 2.00 mm/sec)

The cylindrical shape of the cylindrical threaded tool results in the largest size, and the threads further augment effective tool-workpiece contact area. Frictional heat generated by cylindrical threaded tool will be largest, whereas frictional heat produced by the T tool will be the lowest because to its minimal surface area.

$$Q = \frac{2}{3} \mu \omega \frac{F}{v R_s^2} [(R_s^3 - R_p^3)(1 + \tan \alpha) + R_p^3 + 3R_p^2 H_p] \pi r^2 \quad (7)$$

Figure 3 presents comparison of coefficient of friction, X-force distribution, Z-force, and torque, for each tool utilizing the optimum process parameters (1200 rpm, 2.00 mm/sec).

$$T = 1/12 \pi \mu P D^3 \quad (15)$$

$$P = 4N/(\pi D^2) \quad (8)$$

From Eqn. (2) and (3)

$$T = 1/3 \mu D N \quad (9)$$

The coefficient of friction were,

$$\mu = 3T/DN \quad (10)$$

where, μ = Friction coefficient $D = 2R$ (Tool radius), P = Contact Pressure, N = Normal Pressure, T = Torque, ω = Angular velocity of tool, R_s = Shoulder radius of the tool, R_p = Pin radius of the tool, H_p = Pin Height, α = Tool Shoulder cone angle, F = Axial Force applied, Q = Heat generation rate / Energy input (W), v = Transverse speed / feed rate

Fig 3a demonstrates that nearly all the tools have a consistent torque distribution. The initial torque for the CT were around 36 N·m, decreasing 9 N·m by conclusion of weld. The torque for the T is approximately 10 N·m and 8 N·m. A taper threaded tool (TT) decreases from 32 N·m to 10 N·m. The first elevated torque values are associated with plastic deformation and reduced heating of workpiece, since it is not adequately heated at the outset. A greater reduction at torque values for Taper threaded indicates its superior capacity deform material, attributable to both its taper shape and threading.

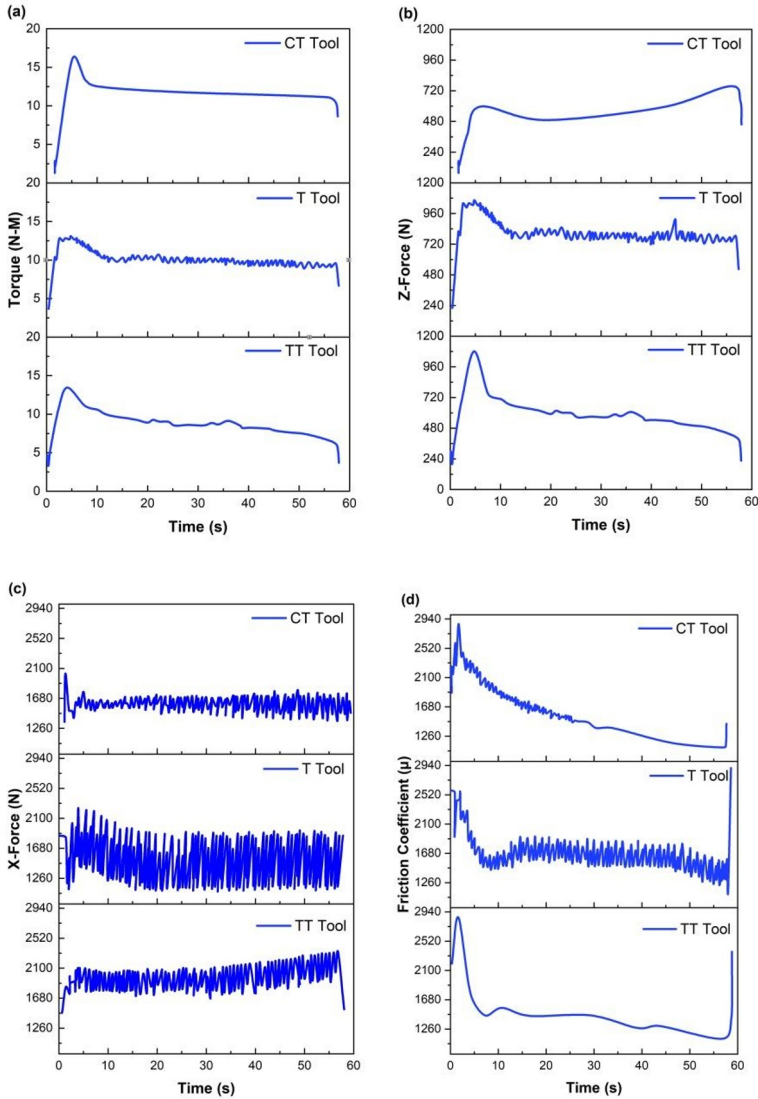


Fig. 3.(a) Distribution of torque for different tool geometries. (b) Distribution of Z-force for different tool geometries. (c) Distribution of X-force for different tool geometries. (d) Distribution of friction coefficient for various tool geometries.

The progressive decrease in pin diameter directs the material flow farther downward, further enhanced by threads. However, the T tool lacks threads, and the cylindrical threaded tool possesses cylindrical form, leading to an increased volume of material deformation. In prior investigations that, the FSW of dissimilar AA6082 and AA2024 alloys was optimized. The study found that welding speed was the most influential parameter for both square and cylindrical threaded tool pins, improving tensile strength [24].

The Z-force were downward vertical force exerted by tool shoulder. The Z-axis mode of Friction Stir Welding, downward vertical force were contingent upon plunge depth relative to top surface of resistance and weld plate exerted by material underneath the shoulder. Tool pin is inclined at 3° and moves with weld line. The tilt generate transverse force that will elevate the distorted material. This increase resistance exerted by material against tool shoulder's inclination to retain their fixed Z-axis. Z-force also influences heat input and directly proportionate relationship. An elevated magnitude of Z-force lead to augmented heat, which may further contribute to deformation. Figure 4b illustrates distribution of Z force escalates from 5000 to 7000 N for the cylindrical threaded tool instrument. The augmentation of Z-force for cylindrical threaded tool illustrates its incapacity to bend material and position it beneath shoulder behind tool efficiently as welding progresses. This leads to heightened flash welding advances. A reduction in Z-force is noted for the taper tool, which experiences a minor increase after 40 seconds. Additionally, a variation at Z-force values is noted during welding process. This illustrates instability of downward force exerted by tool. This could be due to misalignment between the tool and the workpiece. Nonetheless, a tiny layer of flash is also seen on the T tool. The initial force exerted by the Taper threaded tool surpasses that of the other tool, attributable to reduced heat generation from the smaller pin size and heightened friction from the threads. Distribution of X-force indicates that fluctuations of X-force are more consistent at Taper threaded tool compared to the cylindrical threaded tool, where they exhibit a progressive increase.

The increased drop at X-force for T tool indicates challenge at material flow, despite torque achieved being relatively lower. Torque is produced as a result of the tool's rotation into workpiece. The shoulder diameter were three times more than that of the pin. Consequently, influence of the shoulder at torque generation far surpasses that of the pin. X-force represents resistance exerted by workpiece material in response to tool movement. Consequently, the Taper threaded tool pin must traverse less distorted material. This combination results in slippage between the tool and workpiece, leading to increased fluctuations in the Taper threaded tool. The fluctuation in the cylindrical threaded tool is minimal initially but progressively escalates with time, indicating a corresponding increase in flow stress. Fig. 3d illustrates distribution of the friction coefficient at welding process. FC for three tools diminishes welding progresses. The friction coefficient for the cylindrical threaded tool diminishes progressively during welding. The friction coefficient of Tool T initially decreases but thereafter climbs significantly, exhibiting visible fluctuations as the tool advances. It shows that the T tool experiences significant slippage during welding. The fluctuation for the T tool is also seen in X force (Fig. 4c). This attributed to reduced thermal input from T tool, leading to diminished material deformation. It is also evident that using the T tool, forces and torque are relatively lower, further indicating that the material experiences less deformation. For the Taper threaded tool, the friction coefficient initially declines dramatically and subsequently remains stable throughout the welding process. It indicates that the degree of slip among workpiece and tool interfaces in the Taper threaded tool were minimal. The initial peak torque value for the cylindrical threaded tool is around 15 N-m, with a friction coefficient of 0.5, whereas the Z-force were roughly 4000 N. The T tool has a torque of 12 N-m, a coefficient of 0.31, and a force of 8000 N, respectively.

Utilizing the Taper threaded tool, the values are approximately 13 N·m, 0.5, and 5000 N. The motor imparts torque to workpiece to induce angular deformation at material. As reported in previous studies, the effects of programmed torque (PT) and feed rate (FR) on torque variation in FSW of AA6061-T6 using a Taguchi L9 design. The optimal parameters of 45 Nm PT and 100 mm/min FR resulted in minimal torque variation during welding [25]. Friction forces at tool-workpiece will counteract this angular distortion. This necessitates a greater torque for deformation, leading to an abrupt initial rise in torque. As welding progresses, the material softens Z-forces and frictional heat, resulting in increased plastic deformation, which leads to a reduction in both torque and the friction coefficient.

4.2. Evaluation of mechanical characteristics

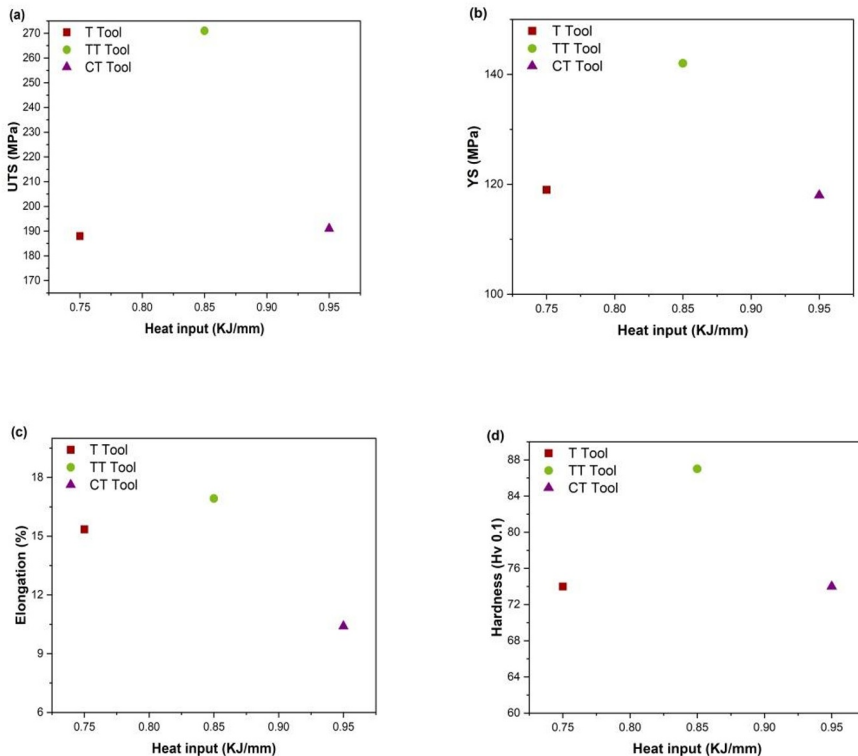


Fig. 4. A comparison of (a) Ultimate tensile strength (b) yield strength (c) Percentage of elongation (d) Hardness at 1200 rpm and 2.00 mm/sec speed

Figures 4 and 5 indicate that the Taper threaded tool has superior tensile characteristics and hardness with a UTS of 271 MPa, YS of 142 MPa, a hardness of 16.92 Hv 0.1 and a percentage elongation of 87%. The cylindrical threaded tool tool has lowest mechanical parameters, with a UTS of 188 MPa, YS of 119 MPa, elongation percentage of 15.35%, and hardness of 79 Hv0.1, based on the optimal parameter settings of 1200 rpm and 2.00 mm/sec. In previous studies, friction Stir Welding (FSW) parameters for AA6061 and AA5083 alloys using hybrid soft computing techniques. The optimization improves ultimate tensile strength

(269.544 MPa), yield strength (211.121 MPa), and elongation (17.127%), enhancing FSW performance for manufacturing industries [26]. Hall-Petch relation indicates that more refined grain size distribution enhances tensile characteristics. Furthermore, refined distribution of precipitates enhances mechanical characteristics of aluminum with both distribution of precipitate and grain size being contingent upon heat generation and degree of deformation. A greater heat input lead to the coarsening of nugget grains and precipitates. A greater deformation of the workpiece may facilitate the development of smaller grains and the reduction of precipitate size. For the T tool, both heat and restricted dislocation movement are factors. The input in FSW and deformation of workpiece were very minimal, indicated by force and torque values (0.32 KJ/mm, 12 N-m, 7000 N, 1145 N). The cylindrical threaded tool tool has largest heat input (0.32 KJ/mm) among tools; nevertheless, its force and torque values are comparatively lower (12.11 N-m, 5333 N, 1156 N). The heat generation of Taper threaded tool (0.96 KJ/mm) surpasses that of the T tool; however, degree of deformation achieved were highest among all tools, as indicated by the force and torque (13 N-m, 8000 N, 5000 N). The factors aid Taper threaded tool at enhanced precipitate distribution and achieving a finer grain size, which in turn resulted at raised mechanical characteristics (1200 rpm, 2.00 mm/sec).

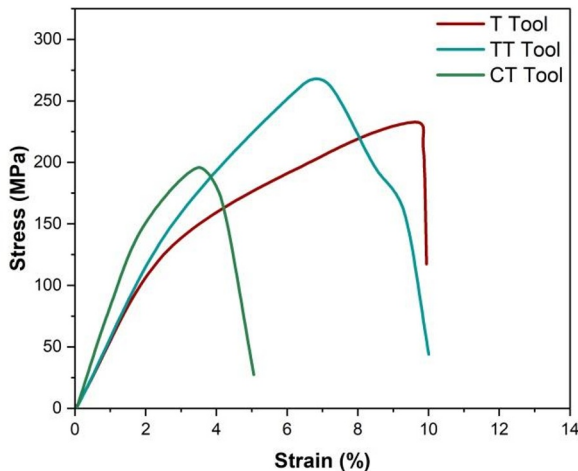


Fig. 5 Stress- strain for various tool (1200 rpm,2.00 mm/sec)

5. Conclusions

This research aims to identify optimal tool geometry from selection tools FSW of AA 5083 T6, (yield strength, ultimate tensile strength, hardness and percentage elongation) while also examining the force and torque characteristics of each tool, which represent tool-workpiece interactions. It has been determined that the Taper threaded tool is most appropriate for current inquiry.

- A comparison of the optimum outcomes for all tool geometries indicates that the TT tool exhibits superior qualities (YS-142 MPa, UTS-271 MPa, hardness-87 Hv0.1, percentage elongation-16.92%) compared to other two tools.

- For TT, enhancements of 22.68% and 11.45 % at UTS were noted in comparison to cylindrical threaded tool and T tools.
- The Taper threaded tool exhibits the maximum torque, X-force, and Z-force when evaluated against other tools under optimal parameters. An enhancement of 16.07% and 2.37% at torque values is observed for the Taper threaded tool in comparison to the cylindrical threaded tool and T tool.
- Fluctuation at Z-force were observed at cylindrical threaded tool. The distribution of Xforce were relatively more uniform and stable for Taper threaded. A greater degree of X-force variation were noted for Taper tool. The coefficients of friction for T, Taper threaded, and cylindrical threaded tool are 0.242, 0.227, and 0.370, respectively.

References

- [1] N. J. Vignesh et al., “ENHANCING AA5083/MgAZ31B PROPERTIES VIA FRICTION STIR WELDING,” *Surface Review and Letters*, vol. 32, no. 10, (2025), doi: 10.1142/S0218625X24501282.
- [2] C. Swain, A. Shukla, and K. Badheka, “Influence of multi-fluted tool pin geometries on mechanical and microstructural characteristics of AA5083 aluminum alloy Friction stir welds,” *Welding International*, (2025), doi: 10.1080/09507116.2025.2599884.
- [3] P. S. Kumar and M. S. Chander, “Effect of tool pin geometry on friction stir welded dissimilar aluminium alloys - (AA5083 & AA6061),” *International Journal of Mechanical Engineering and Technology*, vol. 9, no. 647–653, pp. 647–653, (2018) , [Online]. Available:<https://www.scopus.com/inward/record.uri?eid=2-s2.0-85059231185&partnerID=40&md5=7be1096eb09349334bab205c9be2c04d>
- [4] E. C. P. Nidumolu, R. K. Pittala, and B. Yelamasetti, “A comparative study of microstructure development, corrosion resistance and mechanical properties of dissimilar AA5083–AA6082 weldments produced by CMT, FSW and TIG welding processes,” *Welding International*, vol. 40, no. 1, pp. 1–10, (2026), doi: 10.1080/09507116.2025.2553812.
- [5] D. Vinodh and N. Natrayan, “Integration of ceramic reinforcements in AA5083 composites for enhanced mechanical and thermal properties in friction stir welding,” *Engineering Research Express*, vol. 7, no. 3, (2025), doi: 10.1088/2631-8695/ade9f0.
- [6] S. Arora, “EFFECT OF POST PROCESSING TIME INTERVAL BETWEEN TIG WELDED AND FRICTION STIR PROCESSING OF ALUMINIUM JOINT,” *Transactions of the Royal Institution of Naval Architects Part A: International Journal of Maritime Engineering*, vol. 167, no. A3(S), (2025), doi: 10.5750/ijme.v167iA3(S).1667.
- [7] N. Kothandam, L. Lenin, B. Senthamarakannan, and P. Yogaraj, “Analyzing the Influence of Tool Plunge Depth and Frictional Heat Generation in Friction Stir Welding of Scandium-Modified Dissimilar Aluminum Alloys,” *Transactions of the Indian Institute of Metals*, vol. 78, no. 5, (2025), doi: 10.1007/s12666-025-03581-3.
- [8] O. Muribwathoho, V. Msomi, and S. Mabuwa, “Optimization of FSP parameters in fabricating AA5083/Coal composites using Taguchi method,” *Engineering Research Express*, vol. 7, no. 1, (2025), doi: 10.1088/2631-8695/ada41a.
- [9] M. Mothilal and A. Kumar, “Supervised Machine learning models for predicting mechanical properties of dissimilar friction stir welded AA7075-AA5083 aluminum alloys,” *Measurement (Lond)*, vol. 246, (2025), doi: 10.1016/j.measurement.2025.116653.
- [10] O. Muribwathoho, V. Msomi, and S. Mabuwa, “Optimizing FSP Parameters for AA5083/SiC Composites: A Comparative Analysis of Taguchi and Regression,” *Metals (Basel)*, vol. 15, no. 3, (2025), doi: 10.3390/met15030280.

- [11] S. Charonerat, T. Phatungthane, and C. Summatta, "Optimizing friction stir welding parameters for enhanced mechanical properties of dissimilar aluminum alloys AA5083 and AA6063: A Taguchi approach," *International Journal of Applied Science and Engineering*, vol. 22, no. 3, (2025), doi: 10.6703/IJASE.202509_22(3).006.
- [12] S. Gadakh and C. Nayak, "Multi-response optimization of process parameters for weld performances during underwater friction-stir welding of dissimilar aluminum alloys AA6063-T6 and AA5083-H32," *J. Adhes. Sci. Technol.*, vol. 39, no. 19, pp. 2985–3008, (2025), doi: 10.1080/01694243.2025.2525995.
- [13] P. Kumar and S. Sharma, "Influence of FSW Process Parameters on Formability and Mechanical Properties of Tailor Welded Blanks AA6082-T6 and AA5083-O Using RSM with GRA-PCA Approach," *Transactions of the Indian Institute of Metals*, vol. 74, no. 8, pp. 1943–1968, (2021), doi: 10.1007/s12666-021-02255-0.
- [14] S. Sampath, "Experimental investigation and multi-objective optimization of cryogenic Friction-stir-welding of AA2014 and AZ31B alloys using MOORA technique," *Mater. Today Commun.*, vol. 33, (2022), doi: 10.1016/j.mtcomm.2022.104937.
- [15] S. S. Parkhe and R. J. Patil, "Experimental Investigation and Analysis of Friction Stir Welded Aluminium AA3103 Joint by Taguchi Approach," *Journal of The Institution of Engineers (India): Series D*, (2026), doi: 10.1007/s40033-025-00979-7.
- [16] M. Kolli, C. Sunnapu, and N. R. Nageswara Rao, "Multi-response optimization of friction stir welding process parameter of AA 5083 with Taguchi-VIKOR approach," *Journal of Engineering and Applied Science*, vol. 72, no. 1, (2025), doi: 10.1186/s44147-024-00572-x.
- [17] H. C and S. Chakraborty, "Microstructure evolution and mechanical characterization of dissimilar material (AL6063-T4 and MG AZ31B) in friction stir welding," *Interactions*, vol. 246, no. 1, (2025), doi: 10.1007/s10751-025-02324-6.
- [18] V. Viswanathan, A. K. Babuchellam, V. Vimala, and M. Selvaraju, "Optimizing underwater friction-stir welding parameters for AA356/SiC composites using CoCoSo and MEREC: enhancing joint performance and quality," *Revista Materia*, vol. 30, (2025), doi: 10.1590/1517-7076-RMAT-2024-0948.
- [19] R. Srinivasan, A. Rajakannu, S. Rajesh, J. S. Babu, G. Dinesh, and M. Selvaraju, "Friction Stir Additive Manufacturing of AA7075/Al₂O₃ and Al/MgB₂ Composites for Improved Wear and Radiation Resistance in Aerospace Applications," *Journal of Environmental Nanotechnology*, vol. 14, no. 1, pp. 295–305, (2025), doi: 10.13074/jent.2025.03.2441017.
- [20] D. Dinesh Kumar et al., "Study of Microstructure and Wear Resistance of AA5052/B4C Nanocomposites as a Function of Volume Fraction Reinforcement to Particle Size Ratio by ANN," *J. Chem.*, vol. (2023), doi: 10.1155/2023/2554098.
- [21] Y. Zhang, K. Zhang, T. S. Satish Kumar, F. Alimova, S. Mehrez, and S. S Albuhamdan, "Control of microstructure, tribological and mechanical properties in friction stir processed of AA5083 matrix composites reinforced with NbMoTaTiNi refractory high-entropy particles by using a newly designed tool," *J. Alloys Compd.*, vol. 1044, (2025), doi: 10.1016/j.jallcom.2025.184524.
- [22] S. D. Kumar and R. Pugazhenthii, "Achievement of Optimum Characteristics of Friction Stir Welded Joints with Varied Process Parameters," *International Journal of Vehicle Structures and Systems*, vol. 15, no. 5, pp. 618–622, (2023), doi: 10.4273/ijvss.15.5.06.
- [23] M. H. Saad, B. M. Darras, and M. A. Nazzal, "Evaluation of Welding Processes Based on Multi-dimensional Sustainability Assessment Model," *International Journal of Precision Engineering and Manufacturing - Green Technology*, vol. 8, no. 1, pp. 57–75, (2021), doi: 10.1007/s40684-019-00184-4.
- [24] D. K. Mohapatra, P. P. Mohanty, and M. Mallik, "Effect of tool profile on tensile and flexural behaviour of dissimilar friction stir welded AA 6082 and AA2024," *Canadian*

Metallurgical Quarterly, vol. 65, no. 1, pp. 34–44, (2026), doi: 10.1080/00084433.2025.2481708.

[25] A. Clark and I. Ragai, “Utilizing Taguchi and ANOVA methods to investigate standard deviation of programmed torque for aluminum 6061-T6 friction stir welding with adaptive torque monitoring and control,” *Manuf. Lett.*, vol. 46, pp. 1–4, (2025), doi: 10.1016/j.mfglet.2025.08.004.

[26] A. Rana, S. Deswal, and N. Hooda, “Hybrid heuristic methods exercising to optimize the friction stir welding process parameters for improving the prepared butt joints mechanical properties,” *World Journal of Engineering*, vol. 21, no. 4, pp. 675–694, (2024), doi: 10.1108/WJE-01-2023-0016.